Depth-Dependent Seabed Properties: Geoacoustic Assessment

Chuangxin Lyu[1]; Junghee Park[2]; and J. Carlos Santamarina, A.M.ASCE[3]

Abstract: Offshore geoengineering requires reliable sediment parameters for analysis and design. This study proposes a robust framework for effective stress-dependent geotechnical and geoacoustic properties for seabed analysis based on geophysical models, new experimental data, and extensive data sets compiled from published studies that cover a wide range of marine sediments and depths. First, effective stress-dependent porosity versus depth profiles are computed using compaction models that are valid for a wide stress range. Then, P- and S-wave velocity data are analyzed in the context of effective stress-controlled density, shear stiffness, and bulk modulus within a Hertzian-Biot-Gassmann framework. Finally, this study selects six distinct "reference sediments" that range from clean sands to high-plasticity clays and assigns self-consistent compaction and shear stiffness properties using well-known correlations reported in the literature in terms of specific surface, plasticity, and grain characteristics. Results show that robust physical models for compaction and stiffness adequately predict depth-dependent geotechnical and geoacoustic properties according to sediment type. The asymptotic void ratio at low effective stress e_L determines the sediment density ρ_o at the sediment–water boundary. New experimental studies show that the characteristic asymptotic sediment density ρ_o at very low effective stress $\sigma_z' \to 0$ controls the high-frequency acoustic reflection used for bathymetric imaging. The proposed analysis of geoacoustic data can be used to obtain first-order estimates of seafloor sediment properties and to produce sediment-type seafloor maps. **DOI: 10.1061/(ASCE)GT.1943-5606.0002426.** *This work is made available under the terms of the Creative Commons Attribution 4.0 International license, https://creativecommons.org/licenses/by/4.0/.*

Author keywords: Seafloor characterization; Sediment property profile; Reflection coefficient.

Introduction

Seafloor properties are critical to offshore geotechnical engineering, including foundations and anchors, piping and transmission line projects, the analysis of landslides, geological mapping and the interpretation of marine seismic data, drilling projects, marine landfills, deep-sea mining, and environmental assessment. These projects require soil models that are applicable to a wide range of effective stress.

Depth-dependent geotechnical parameters such as density ρ (kg/m^3), effective stress (kPa), and shear stiffness (kPa), and geoacoustic parameters such as P- and S-wave velocities V_P and V_S (m/s) display distinct differences among sediment types (Hamilton 1972; Hamilton and Bachman 1982; Jackson and Richardson 2007). Therefore, a geoacoustic seabed assessment can provide noninvasive information relevant to the sediment engineering properties.

Sediment characteristics at very low effective stress near the sediment–water boundary are critical for high-frequency surface reflection measurements and for the interpretation of bathymetric data to eventually produce sediment-type seafloor maps. As the effective stress increases with depth, depth-dependent geoacoustic parameters affect the analysis of layer reflections gathered with lower-frequency systems such as subbottom profilers and marine seismic towed streamer [Note: sediment depths can exceed 3,000 m; see examples in Grant and Schreiber (1990), Wunderlich et al. (2005), Schrottke et al. (2006), and Wang and Rao (2009).] Furthermore, engineered systems can induce a high effective stress, such as gas production from hydrate-bearing sediments (Moridis et al. 2011).

Seafloor acoustic assessment is particularly convenient. Contrary to previous phenomenological approaches, this study builds from the fundamental observation that sediment properties are effective stress-dependent and adopts physics-inspired models to anticipate seafloor characteristics: Terzaghi self-compaction, Hertzian-DLVO stiffness, and Biot-Gassmann bulk stiffness (from published work, including the authors'). The study benefits from an extensive database compiled from the literature (depth-dependent seafloor porosity and wave velocities V_S and V_P), and contributes new data for very low effective stress conditions where information was sparse. Finally, these data are used to address the reflection from the water–sediment interface, which controls high-frequency bathymetric studies. The parameters selected for the various models involved in this study are mutually self-consistent and satisfy well-tested published correlations.

Depth-Dependent Density and Effective Stress

Self-compaction reflects the dependency between effective stress σ_z' and sediment density ρ_s. In this section, an asymptotically correct compaction model is used and the evolution of effective stress σ_z', porosity n, and sediment density ρ_s is investigated for a wide range of sediments in the upper 1,000 m of the sediment column.

Compaction Model: Void Ratio versus Effective Stress

Fig. 1 presents compaction trends for a wide range of soils, from high-plasticity clays to clean sands. Clearly, the sediment void

[1]Ph.D Student, Dept. of Civil and Transport Engineering, Norwegian Univ. of Science and Technology, Trondheim 7491, Norway.

[2]Research Scientist, Earth Science and Engineering, Bldg. 5, King Abdullah Univ. of Science and Technology, Thuwal 23955-6900, Saudi Arabia (corresponding author). ORCID: https://orcid.org/0000-0001-7033-4653. Email: junghee.park@kaust.edu.sa

[3]Professor, Earth Science and Engineering, King Abdullah Univ. of Science and Technology, Thuwal 23955-6900, Saudi Arabia.

Note. This manuscript was submitted on June 9, 2019; approved on August 13, 2020; published online on October 24, 2020. Discussion period open until March 24, 2021; separate discussions must be submitted for individual papers. This paper is part of the ***Journal of Geotechnical and Geoenvironmental Engineering***, © ASCE, ISSN 1090-0241.

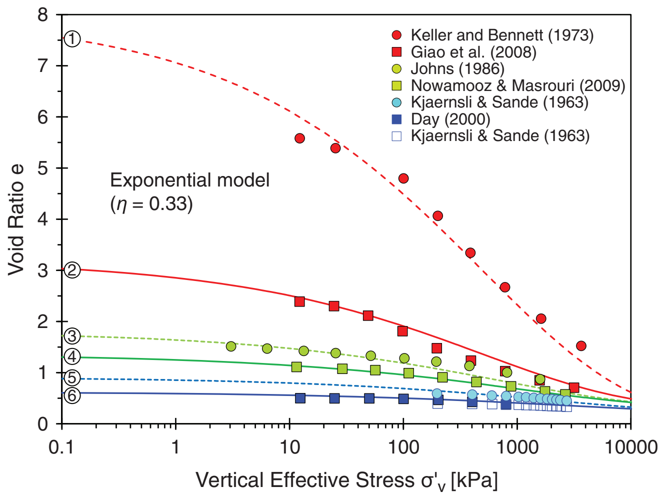

Fig. 1. (Color) Compression curves in terms of void ratio e versus effective stress σ_z'. Data points show data compiled from published studies. Lines correspond to the asymptotically correct exponential compaction model [Eq. (1)]. Table 1 lists sediment constitutive parameters for the six *reference sediments*.

ratio e decreases as a function of the vertical effective stress σ_z', and compressibility increases with sediment plasticity. The compaction trend is nonlinear in the conventional semi-log space, so the classical Terzaghi model $e = e_{1\ \mathrm{kPa}} - C_c \cdot \log(\sigma_z'/1\ \mathrm{kPa})$ fails to satisfy asymptotic conditions at very low and high effective stresses (see also Mesri and Olson 1971; Johns 1986; Burland 1990; Pestana and Whittle 1995; Gregory et al. 2006). In particular, the low effective stress asymptote void ratio e_L must be properly captured because it plays a critical role in high-frequency bathymetric data analysis.

Therefore, this study uses an asymptotically correct exponential compaction model in terms of void ratios e_L at low effective stress ($\sigma_z' \to 0$) and e_H at very high effective stress ($\sigma_z' \to \infty$); then the void ratio e_z at depth z is a function of the vertical effective stress σ_z' (Gregory et al. 2006; Chong and Santamarina 2016):

$$e_z = e_H + (e_L - e_H)\exp\left[-\left(\frac{\sigma_z'}{\sigma_c'}\right)^{\eta}\right] \tag{1}$$

where the model parameter η captures the void ratio sensitivity to effective stress and is often $\eta \approx 1/3$, and σ_c' is the characteristic effective stress so that $(e_z - e_H) = 0.37(e_L - e_H)$ when $\sigma_z' = \sigma_c'$.

Fig. 1 shows exponential compaction trends for six *reference sediments* selected to bound the experimental data. The model parameters correlate with the sediment specific surface, plasticity, and grain shape (Table 1 summarizes the model parameters for the six reference sediments). The scale used in this figure reaches $\sigma_z' = 10$ MPa to test the wide stress range validity of the exponential $e_z - \sigma_z'$ model [Eq. (1)].

The void ratio of sandy sediments at low effective stress e_L reflects the grain size distribution and particle shape (Youd 1973; Cho et al. 2006). At a given relative density D_r, the value of e_L can be estimated from the coefficient of uniformity C_u and particle roundness R^* as $e_L = (0.02 - 0.032 \cdot D_r) + (0.893 - 0.522 \cdot D_r)/C_u + (0.236 - 0.154 \cdot D_r)/R^*$; for example, $e_L = 0.89$ for a sandy sediment with $C_u = 3$, and $R^* = 0.3$ at $D_r = 30\%$.

On the other hand, mineralogy and depositional environment determine the void ratio e_L and the compressibility of *clay-rich sediments* (Palomino and Santamarina 2005; Wang and Siu 2006; Wang and Xu 2007). Assuming an edge-to-face fabric, the value of e_L is a function of the particle slenderness, $e_L = (a-1)/2$ where the slenderness ratio a is equal to the particle length divided by its thickness; for example, kaolinite has $a \approx 10$ and $e_L = 4.5$, while montmorillonite has $a \approx 100$ and $e_L = 50$ (Santamarina et al. 2001). Remolding disturbs the initial fabric and any subsequent diagenesis (Burland 1990; Leroueil 1996; Hong et al. 2012).

Table 1. Select reference sediments. Constitutive parameters for effective stress-dependent compaction model [Eq. (1): model parameter $\eta = 1/3$] and shear stiffness in terms of shear wave velocity [Eq. (5)]. Parameters are self-consistent and satisfy published correlations in terms of specific surface, plasticity, and grain shape

Reference sediment	Compaction model [Eq. (1)]			Shear wave velocity [Eq. (5)]	
	e_L	e_H	σ_c' (kPa)	α (m/s)	β
1	8	0.1	500	22	0.38
2	3.2	0.3	500	33	0.32
3	1.80	0.3	700	58	0.25
4	1.35	0.3	1,000	75	0.23
5	0.91	0.2	2,000	110	0.19
6	0.60	0.2	3,000	146	0.17

Source: Data from Santamarina and Cho (2004), Cha et al. (2014), Chong and Santamarina (2016).

Depth-Dependent Density and Porosity

Consider a thin seabed layer of thickness dz at depth z. Force equilibrium combines with gravimetric-volumetric relations to predict the effective stress gradient $d\sigma_z'/dz$ as a function of the void ratio e_z at depth z (note that gravity $g = 9.81\ \mathrm{m/s^2}$):

$$\frac{d\sigma_z'}{dz} = \rho_w \left[\frac{S_G - 1}{1 + e_z}\right] g \tag{2}$$

where the mineral-specific gravity $S_G = \rho_m/\rho_w$ is the ratio between the mineral and water densities ρ_m and ρ_w. Eq. (1) is inserted in Eq. (2), and the differential equation is solved. The closed-form solution for $\eta = 1/3$ predicts the following effective stress profile σ_z' with depth z (for η = 1/3—See related example for methane hydrate-bearing sediments in Terzariol et al. 2020):

$$z = \frac{(1+e_H)}{(S_G - 1)\rho_w g}\sigma_z' + 3\frac{(e_L - e_H)}{(S_G - 1)\rho_w g}\sigma_c'\left\{\left[\left(\frac{\sigma_z'}{\sigma_c'}\right)^{\frac{2}{3}} + 2\left(\frac{\sigma_z'}{\sigma_c'}\right)^{\frac{1}{3}} + 2\right] \cdot \exp\left[-\left(\frac{\sigma_z'}{\sigma_c'}\right)^{\frac{1}{3}}\right] - 2\right\} \tag{3}$$

Fig. 2(a) shows the effective stress trends for the six reference sediments identified earlier (Fig. 1; Table 1). Effective stress gradients decrease markedly as sediments change from sands to high-plasticity clays.

Finally, Eq. (1) is used to compute the void ratio e_z and the sediment density $\rho_s(z)$ as a function of depth z:

$$\rho_s(z) = \rho_w\left[\frac{S_G + e_z}{1 + e_z}\right] \tag{4}$$

Fig. 2(b) shows the change in sediment density ρ_s with depth z. At the sediment–water boundary $z = 0$, sediments experience zero effective stress and the sediment density is the asymptotic value ρ_o defined by $e_{(z=0)} = e_L$ [Eq. (4)]; conversely, the sediment density ρ_s increases toward the value defined by e_H as the sediment depth

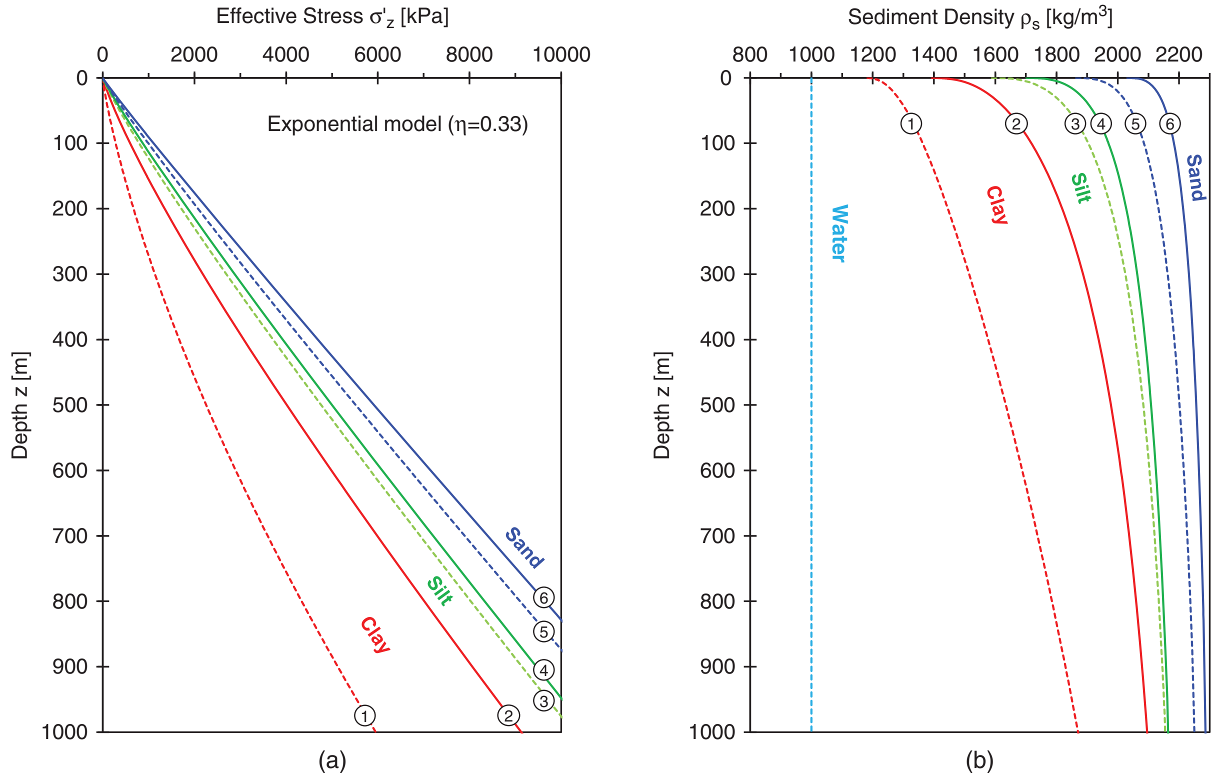

Fig. 2. (Color) Soil state parameters: (a) effective stress σ_z'; and (b) density ρ profiles for different sediment types. Lines correspond to selected *reference sediments* [Eqs. (1)–(4)—constitutive parameters in Table 1].

increases. Once again, the six trends in Fig. 2(b) correspond to the six reference sediments identified in Fig. 1 (parameters in Table 1) and show marked differences in density for sand, silts, and clays in the upper 1,000 m. While remolding by sediment transport can affect the sediment density in shallow accumulations, eventually effective stress-dependent compaction prevails as sediment burial progresses.

Fig. 3 shows the evolution of sediment compaction with depth in terms of porosity $n = e/(1+e)$ for data gathered from published references and the Ocean Drilling Program (ODP) projects. The data set involves normally consolidated sediments (i.e., no overpressure) and relatively homogeneous deposits. Once again, trends correspond to the reference sediments; the 1,000-m depth makes it possible to corroborate the wide stress range validity of the exponential $e_z - \sigma_z'$ model [Eq. (1)]. Some reported so-called sands exhibit high porosities; this may reflect grains with intraparticle porosity [e.g., carbonate sands (Goldhammer 1997)] or incorrect reporting of sandy sediments with high fines content so that fabric formation is fines-dominant. In general, computed trends for the six reference sediments selected earlier follow the field data for the different sediment types. (Note: the six reference sediment trends reflect self-compaction properties according to sediment type; these profiles are not intended to fit any particular data set.) The logarithm of depth used in Fig. 3 helps with exploring near-surface conditions in detail, but trends can be misleading: in linear scale, porosity decreases at a faster rate near the sediment–water interface.

Depth-Dependent P- and S-Wave Velocities

Effective stress determines not only the sediment density ρ_s but also the stiffness of the sediment granular skeleton in the absence of cementation. In turn, stiffness and mass density define P- and S-wave velocities. This section brings together P- and S-wave velocity data compiled from the literature and new experimental data gathered in this study to overcome the scarcity of published data at very shallow depths. Then, the P- and S-wave velocity data are analyzed in the context of effective stress-dependent density, shear stiffness, and bulk modulus.

Experimental Study: P- and S-Wave Velocities at Very Low σ_z'

Devices

The miniature P- and S-wave measurement probes built for this study involve split tubes to minimize the transmission of vibrations around the tube and boundary-reflected waves (dimension: $\phi =$ 34 mm in diameter and $H = 500$ mm in height). We mount the parallel-type bender elements for S-waves and the piezo disk elements for P-waves at the tip of the split tubes to reduce disturbance effects caused by probe penetration (insets in Figs. 4 and 5). Crystals are coated with silver paint and grounded to prevent electrical crosstalk [details in Lee and Santamarina (2005a)].

Test Procedure

The experimental study involves sediment beds prepared with fine sand, silt, and kaolinite in large-diameter columns to minimize boundary effects during the penetration of the P- and S-wave probes (columns are 300 mm in diameter and 600 mm in height). Table 2 summarizes the sediment index properties. These seafloor analogs form by sedimentation from diluted slurries to prevent gas entrapment and layering (initial water content $\omega >$ 2,000%). All sediments consolidate for 2 weeks. Then P- and S-waves are recorded every 1 or 2 cm (note that signals are stable within a few

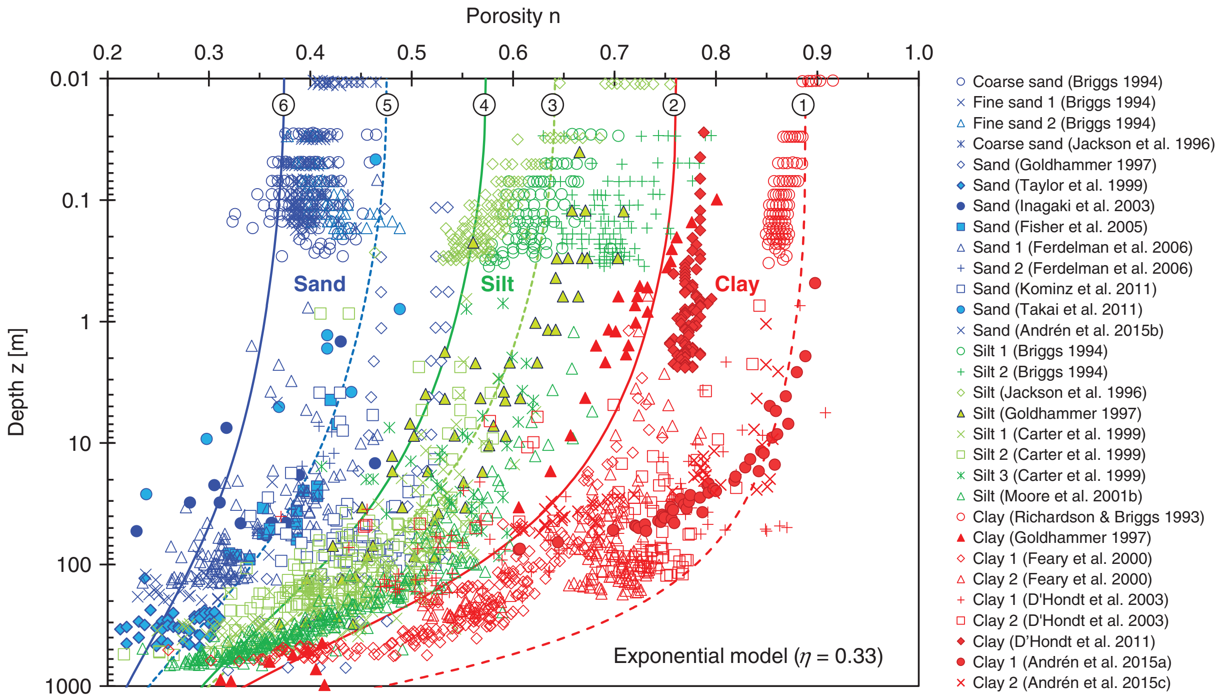

Fig. 3. (Color) Porosity n versus depth z. Data points compiled from published studies. Lines show computed trends for selected reference sediments [Eqs. (1)–(3)—constitutive parameters in Table 1].

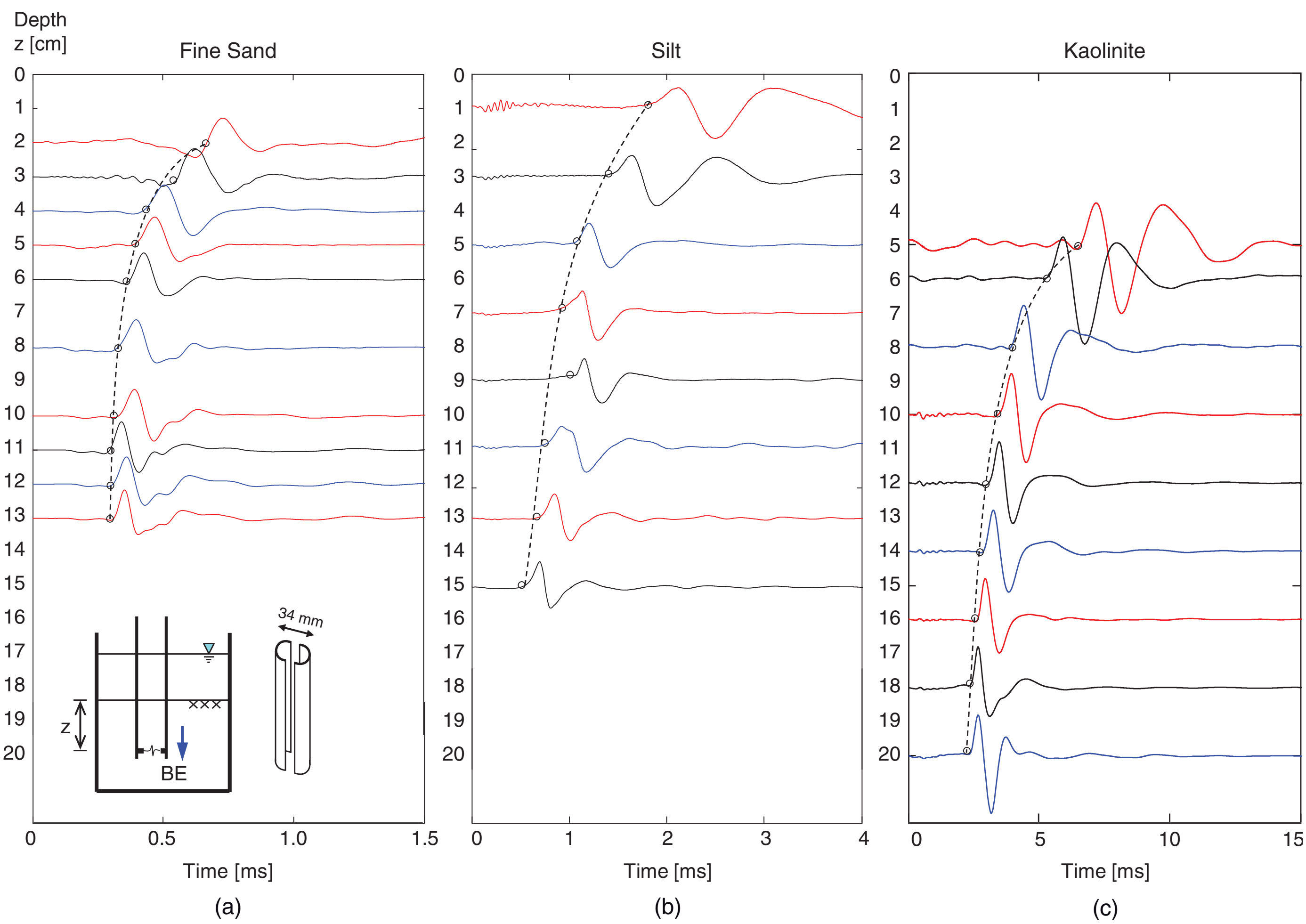

Fig. 4. (Color) Shear S-wave signatures versus depth: (a) fine sand; (b) silt; and (c) kaolinite. The different time scales for the three sediments.

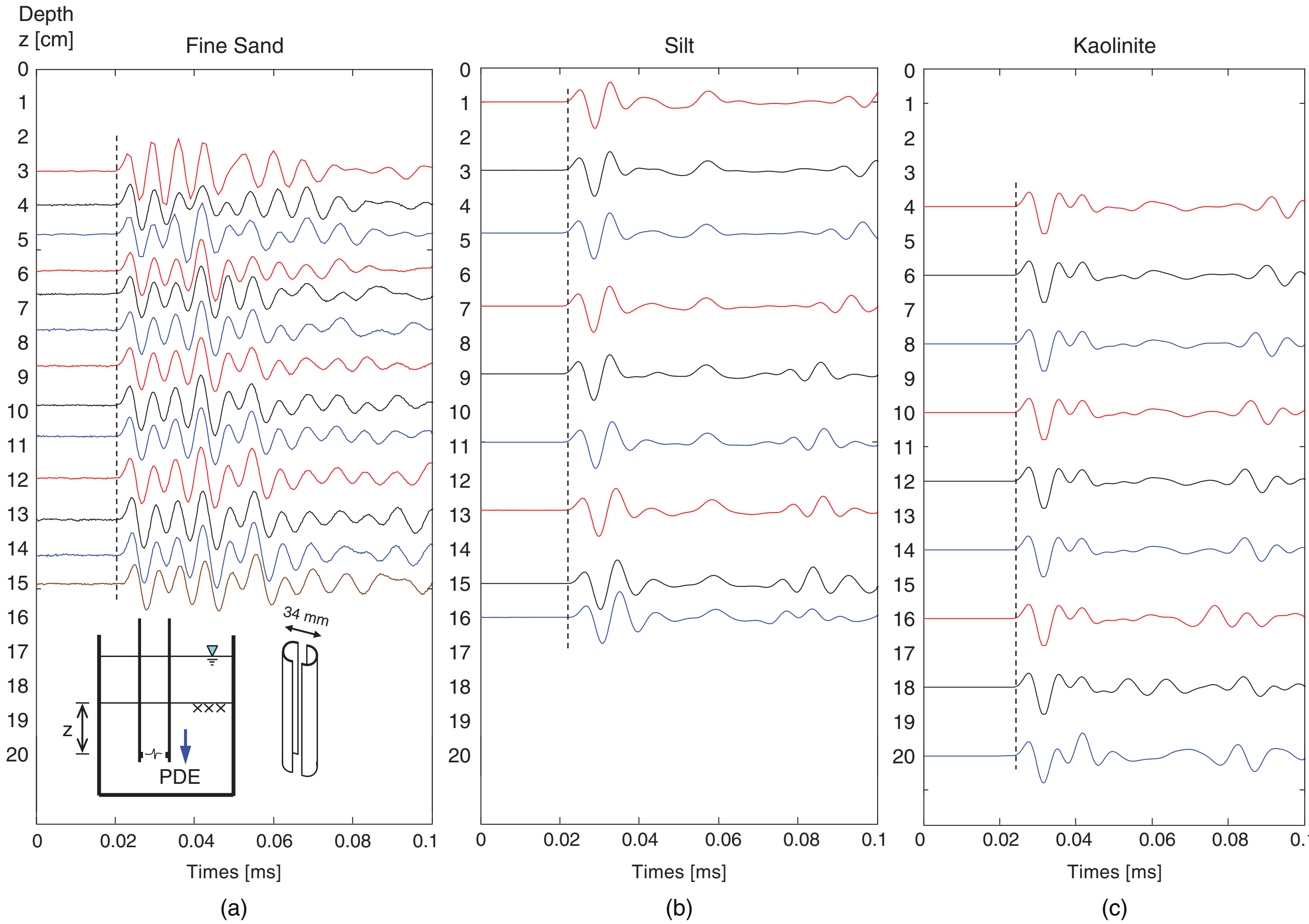

Fig. 5. (Color) Compressional P-wave signatures versus depth: (a) fine sand; (b) silt; and (c) kaolinite. The same time scale for the three sediments.

Table 2. Tested sediments—index properties

Material	Diameter (mm)	Extreme void ratios, e_{max}/e_{min}	Mean grain size d_{50} (mm)	Specific gravity, S_G	Liquid limit (W/B/K)	Specific surface (m^2/g)	RSCS—fines classification
Cobbles	10–20	—	15	2.65	N/A	N/A	N/A
Coarse sand	1.0–2.0	0.82/0.59	1.5	2.65	N/A	N/A	N/A
Fine sand	0.075–0.25	0.81/0.45	0.16	2.63	N/A	N/A	N/A
Silt	<0.075	1.50/0.73	1.0×10^{-2}	2.65	N/A	N/A	N/A
Kaolinite (RP2)	<0.075	N/A	3.0×10^{-4}	2.67	67/52/82	33	I-I
Bentonite	<0.075	N/A	5.0×10^{-6}	2.65	302/92/39	544	H-H

minutes after each insertion, as soon as any excess pore-water pressure dissipates).

P- and S-Wave Signatures

Figs. 4 and 5 present P- and S-wave signatures gathered at very shallow depths and low effective stress in the sandy, silty, and clayey sediments [field data gathered with a velocity-resistivity probe can be found in Lee et al. (2010) and Yoon and Lee (2010)]. The time to first arrival decreases with depth for S-waves, while the travel time for P-waves is almost constant with depth.

Shear Wave Velocity versus Depth

Fig. 6 plots the measured and collected shear velocity V_S data set. The shear wave velocity increases with depth for all sediments. The effective stress σ_z' determines the sediment shear stiffness G_s in the absence of diagenetic cementation. In fact, the shear wave velocity $V_s = \sqrt{G_s/\rho_s}$ follows a Hertzian-type power relation with effective stress (Roesler 1979):

$$V_s = \alpha \left(\frac{\sigma_z'}{1\ \text{kPa}} \right)^{\beta} \quad (5)$$

The α-factor (m/s) is the shear wave velocity at $\sigma_z' = 1$ kPa, and the β-exponent represents the sensitivity of the shear wave velocity to effective stress. These α-factor and β-exponent reflect the sediment type; in general, higher-specific-surface sediments are more compressible, exhibit a lower α-factor, and a more pronounced increase in shear stiffness with stress, i.e., a higher

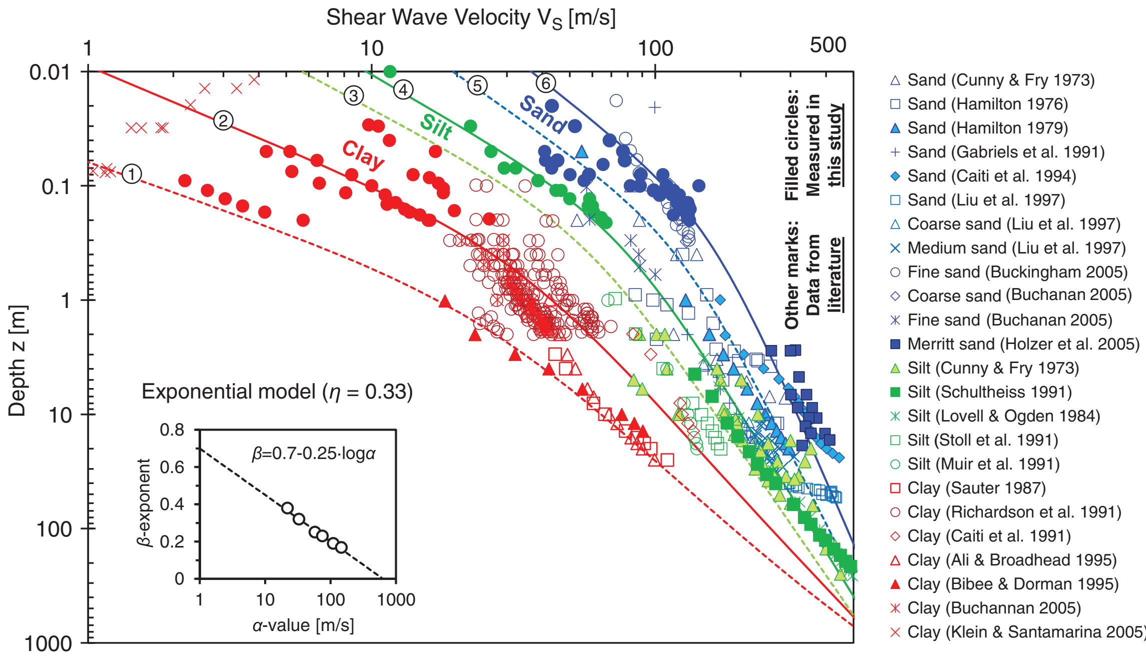

Fig. 6. (Color) S-wave velocity V_S versus depth z. Filled circles indicate measurements gathered in this study, and other symbols are data collected from published studies (frequency range: ~2.5 Hz to 5 kHz). Lines represent the power trend between S-wave velocity V_S and effective stress σ_z' for selected reference sediments [Eq. (5)—constitutive parameters in Table 1].

β-exponent. Thus, there is an inverse relationship between the α-factor and β-exponent, as observed for a wide range of soils: $\beta = 0.7 - 0.25\log[\alpha/(\mathrm{m/s})]$ [see database in Cha et al. (2014)].

The shear wave velocity for fines-controlled sediments is affected by pore fluid chemistry (Klein and Santamarina 2005; Kang et al. 2014). Furthermore, diagenesis may affect both fine- and coarse-grained sediments. In particular, synsedimentary diagenesis makes deeper and older sediments stiffer than remolded specimens at the same effective stress; in this case, the shear wave velocity increases with depth owing to the effective stress and diagenesis and the field β-exponent will be higher than for remolded specimens in the laboratory [see data in Ku (2012) and Ku et al. (2017)].

Table 1 lists α and β values for the six reference sediments, inferred from their compressibility (refer to Part 1). Effective stress profiles from Eq. (3) combine with Eq. (5) to predict the shear wave velocity trends shown in Fig. 6. The computed V_S profiles for the six reference sediments exhibit trends similar to those in the data and successfully bound laboratory and field measurements. Once again, the shear wave velocity increases rapidly with depth in linear-linear scale [power trend in Eq. (5)].

P-Wave Velocity versus Depth

The sediment shear modulus $G_s = \rho_s \cdot V_S^2$ is a function of the shear wave velocity and the sediment mass density [Figs. 6 and 2(b)]. At small strains, the bulk modulus B_{sk} of the sediment granular skeleton is related to the shear modulus as

$$B_{sk} = G_s \frac{2(1+\nu_{sk})}{3(1-2\nu_{sk})} \tag{6}$$

where the small-strain Poisson's ratio of the soil skeleton is $\nu_{sk} \approx 0.15$. The bulk modulus of the water-saturated sediment B_s depends on its porosity n and is a function of the bulk stiffness of the skeleton B_{sk}, water B_w, and mineral B_m:

$$B_s = B_{sk} + \left(\frac{n}{B_w} + \frac{1-n}{B_m}\right)^{-1} \tag{7}$$

On the other hand, the sediment density ρ_s (kg/m^3) is a function of the water ρ_w and mineral ρ_m densities and the sediment porosity n:

$$\rho_s = n\rho_w + (1-n)\rho_m \tag{8}$$

Finally, the low-frequency Biot-Gassmann P-wave velocity V_P (m/s) for soft marine sediments is [from Eqs. (6)–(8)]

$$V_p = \sqrt{\frac{B_s + \frac{4}{3}G_s}{\rho_s}} = \sqrt{\frac{\left[\frac{2(1+\nu_{sk})}{3(1-2\nu_{sk})} + \frac{4}{3}\right](n\rho_w + (1-n)\rho_m)V_s^2 + \left(\frac{n}{B_w} + \frac{1-n}{B_m}\right)^{-1}}{n\rho_w + (1-n)\rho_m}} \tag{9}$$

Fig. 7 shows the estimated P-wave velocity profiles versus depth for the six selected reference sediments. These trends take into consideration the depth-dependent shear wave velocity and porosity profiles computed earlier (Figs. 3 and 6). The figure includes a comprehensive data set gathered from published studies and our own experimental data (Fig. 5). Trends for the reference sediments adequately resemble the data for different sediments (not intended to fit any specific data set).

The water bulk modulus B_w controls the P-wave velocity in saturated soft sediments near the seafloor (pure water $V_P = 1{,}480$ m/s; seawater $V_P = 1{,}531$ m/s), and changes in P-wave velocity are relatively minor in the upper tenths of meters in clayey deposits. In fact, the P-wave velocity may fall below that of water when the increase in mass density is faster than the increase in skeletal stiffness in plastic sediments at shallow depth. (Note: This

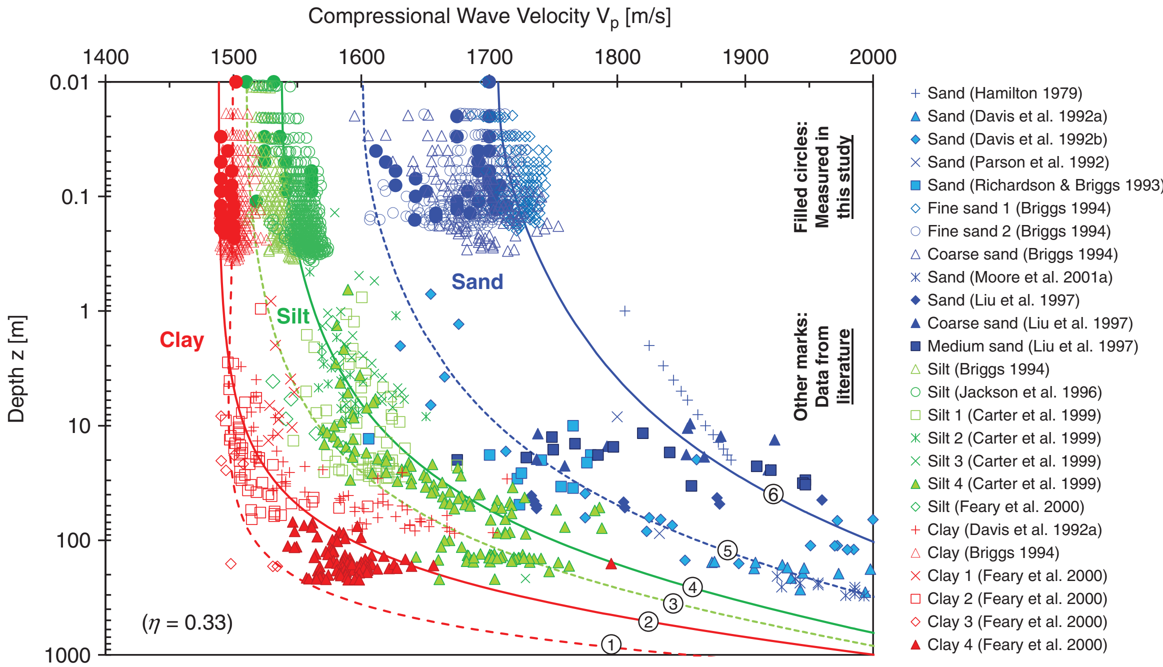

Fig. 7. (Color) P-wave velocity V_P versus depth z. Filled circles indicate measurements gathered in this study, and other symbols are data collected from published studies (frequency range: 120–400 kHz). Lines show Biot-Gassmann P-wave velocity for selected reference sediments [Eq. (9)—bulk modulus: mineral $B_m = 45$ GPa, gas-free water $B_w = 2.37$ GPa. Density: water $\rho_w = 1{,}024$ kg/m^3, mineral $\rho_m = 2{,}680$ kg/m^3]. Small-strain Poisson's ratio of soil skeleton $\nu_{sk} = 0.15$. Porosity $n = e_z/(1+e_z)$ from integration of Eqs. (1) and (4). [Shear wave velocity V_S at depth z from Eq. (5)—parameters in Table 1.]

explains the crossing of the two trends for clayey sediments in Fig. 7.)

The P-wave velocity relaxation in sediments leads to the following ratio between the Biot high-frequency P-wave velocity $V_{P\infty}$ and the low-frequency P-wave velocity V_{Po} computed in Eq. (9) (Santamarina et al. 2001):

$$\frac{V_{P\infty}}{V_{P_0}} = \sqrt{\frac{[n\xi + n^2(S_G - 2) - n^3(S_G - 1)][S_G(1-n) + n]}{\xi n S_G(1-n) + n^2(\xi - 1)}} \quad (10)$$

where ξ is a tortuosity factor. The velocity ratio is approximately $V_{P\infty}/V_{Po} \approx 1.05$ [Eq. (10), porosity $n \approx 0.4$, and tortuosity factor $\xi = 2$]. Fig. 8 shows the effect of porosity n on P-wave velocities V_{Po} and $V_{P\infty}$. Data points are values measured for "undisturbed samples" recovered from the seafloor (Richardson and Briggs 1993). The low-frequency P-wave velocity V_{Po} [red trend—Eq. (9)] and the high-frequency $V_{P\infty}$ (red line) provide lower and upper trends for most of the data shown in Fig. 8 when the skeletal stiffness is null, $V_S = 0$ m/s. The central trend is best predicted with Eq. (9) for a shear wave velocity $V_S \approx 250$ m/s, which could result from either diagenesis or suction effects when recovered specimens are tested in air (dashed line).

Heterogeneity

Data plots in the global depth z-scale include changes in stratigraphy with depth [e.g., ODP holes in Leg 139–Juan de Fuca Ridge (Mottl et al. 1994)]. Compaction models make it possible to convert depth into effective stress [Eq. (3)] in order to analyze geoacoustic properties in terms of local effective stress σ_z' [Eqs. (1), (4), (5), and (9)].

Discussion and Implications

In the previous two sections, a formulation and supportive database were constructed for depth-dependent geotechnical properties (density ρ_s, porosity n, shear stiffness $G_s = \rho_s \cdot V_S^2$) and geoacoustic properties (V_S and V_P) as functions of sediment type. The model parameters selected for the reference soils satisfy well-proven correlations with specific surface, plasticity, and grain shape. Here, the implications for bathymetric studies and seafloor sediment characterization are explored and crucial parameters that require further investigation are identified.

High-Frequency Reflection—Enhanced Bathymetric Analysis

The asymptotic conditions at the water–sediment interface $z \to 0$ are of particular interest because they determine the reflectivity in high-frequency bathymetric studies. A well-controlled reflection data set was created from sediment beds formed with bentonite, kaolinite, silica flour, fine sand, coarse sands, and cobbles. Table 2 summarizes the selected sediments and their index properties. The chamber is 300 mm in diameter and 600 mm in height. All tests are repeated with two crystal pairs to measure reflections at frequencies $f_r = 160$ and 500 kHz [see details on transducer performance in Lee and Santamarina (2005b)]. The spacing between the source and receiver crystals is 20 mm in both cases.

Fig. 9 presents P-wave signatures reflected from a submerged steel plate placed at different depths. The multiple reflection events confirm phase inversion at the air–water interface and the combined effects of geometric spreading and material attenuation. The energy in the first reflection is used as a reference.

Fig. 10 presents the first reflection from the steel plate in comparison to reflections from the fine sand, silt, kaolinite, and

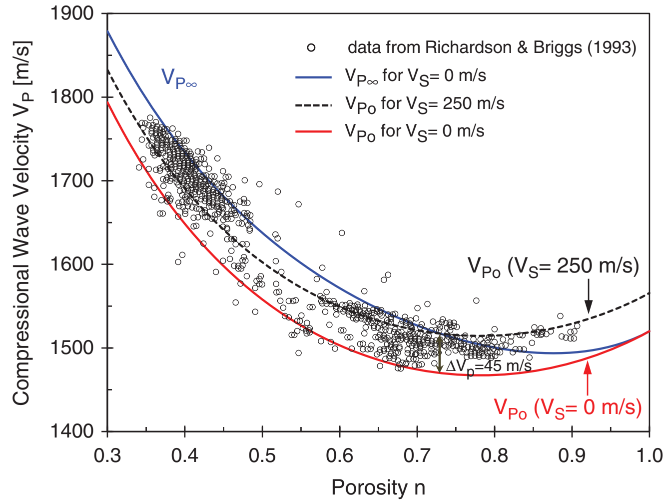

Fig. 8. (Color) Compressional wave velocity V_P as a function of porosity n. Data points from Richardson and Briggs (1993) include clays, silty clays, silty sands, fine sands, and coarse sands (frequency = 400 kHz). Black and red lines show calculated low-frequency Biot-Gassmann P-wave velocity (for $V_S = 0$ and 250 m/s); blue line is an estimate of Biot's high-frequency P-wave velocity $V_{P\infty}$ for sediments with $V_S = 0$ [Eq. (9)]—bulk modulus: mineral $B_m = 45$ GPa, gas-free water $B_w = 2.37$ GPa. Density: water $\rho_w = 1{,}024$ kg/m^3, mineral $\rho_m = 2{,}680$ kg/m^3. Small-strain Poisson's ratio of soil skeleton $\nu_{sk} = 0.15$.

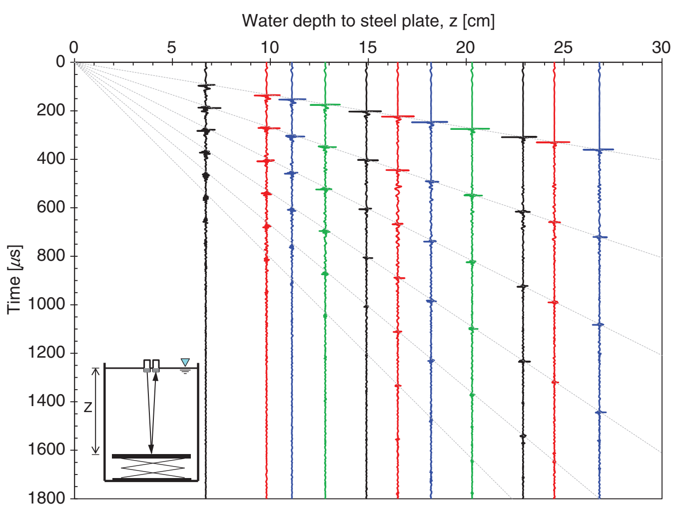

Fig. 9. (Color) Reflection signatures. Target: steel plate at different water depths. Phase reversal occurs after every reflection at air–water interface.

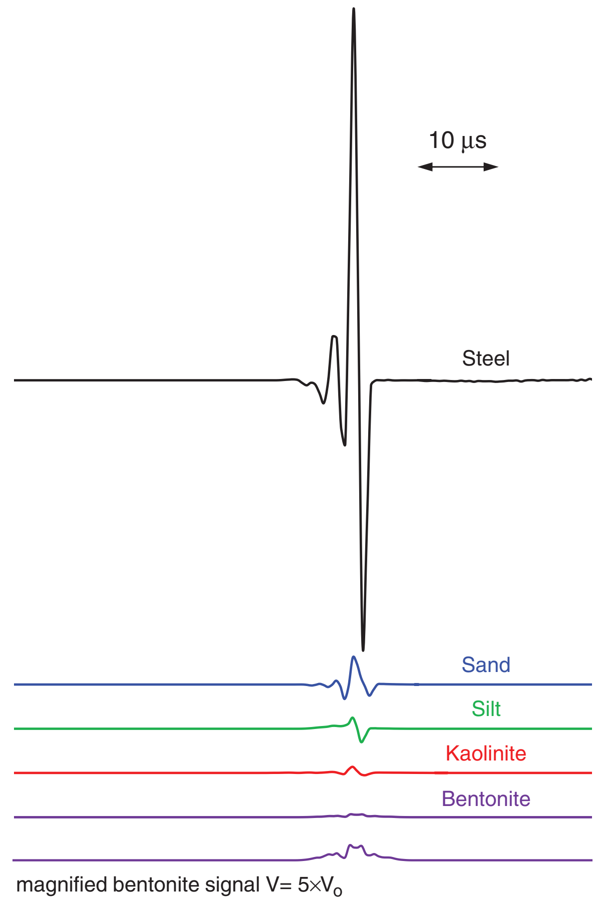

Fig. 10. (Color) Reflection signatures: steel plate and various sediments tested in this study: fine sand, silt, kaolinite, and bentonite. Hanning window around reflection used for energy calculations.

bentonite beds, all at the same water depth. Clearly, the reflection amplitude is strongly related to sediment type and the ensuing asymptotic properties at very low effective stress $\sigma_z' \to 0$ near the water–sediment interface $z \to 0$. The mismatch in acoustic impedance $Z = \rho \cdot V_P$ between the water column and the reflector defines the energy E in the reflected signal, i.e., the reflection coefficient. Then the relative reflection coefficient RR between a sediment bed and the steel target is

$$RR = \frac{E_s}{E_{st}} = \left[\frac{(Z_w + Z_{st})(Z_w - Z_s)}{(Z_w - Z_{st})(Z_w + Z_s)}\right]^2 = 1.14 \times \left(\frac{1 - \frac{Z_s}{Z_w}}{1 + \frac{Z_s}{Z_w}}\right)^2 \quad (11)$$

where the subscripts s, w, and st indicate sediment, water, and steel, respectively. The "1.14" factor in the last mathematical expression corresponds to the water–steel interface (steel: $\rho = 7{,}900$ kg/m^3, $V_P = 5{,}900$ m/s; water: $\rho = 1{,}024$ kg/m^3, $V_P = 1{,}531$ m/s). Fig. 11 summarizes the energy-based RR measured for all sediments versus their mean grain size d_{50}. Sandy sediments exhibit the highest reflection coefficient, while the very soft bentonite bed produces the smallest coefficient. [Note that published results corroborate the importance of sediment type on reflectivity, for example, van Walree et al. (2005, 2006) and Snellen et al. (2011); attenuation in Panda et al. (1994); spectral strength in Sternlicht and de Moustier (2003).]

The sediment density ρ_s and P-wave velocity profiles for the six reference sediments explored earlier make it possible to estimate the theoretically computed RR [Eq. (11); refer to Figs. 3(b) and 7 for the sediment ρ_s and V_P]. Fig. 11 shows the theoretical reflection coefficient computed at different sediment depths from $z^* = 3$ to 1,000 mm. The depth $z^* = 3$ mm relates to the wavelength λ at $f_r = 500$ kHz, while the impedance at depth $z^* = 150$ mm may be more relevant for the operating frequency of subbottom profilers $f_r = 10$ kHz. Data trends suggest a slope of approximately 1/4 for the $\log(RR)$ versus the $\log(d_{50})$. The theoretically computed RR at depth $z^* = 3$ mm tracks the experimental data when the mean grain size d_{50} is smaller than 1/10 of the wavelength $\lambda = 3$ mm. Thereafter, the reflection coefficient decreases rapidly (Brillouin zone). Field data gathered with a single-beam echosounder (Snellen et al. 2011) show good agreement with the results presented here

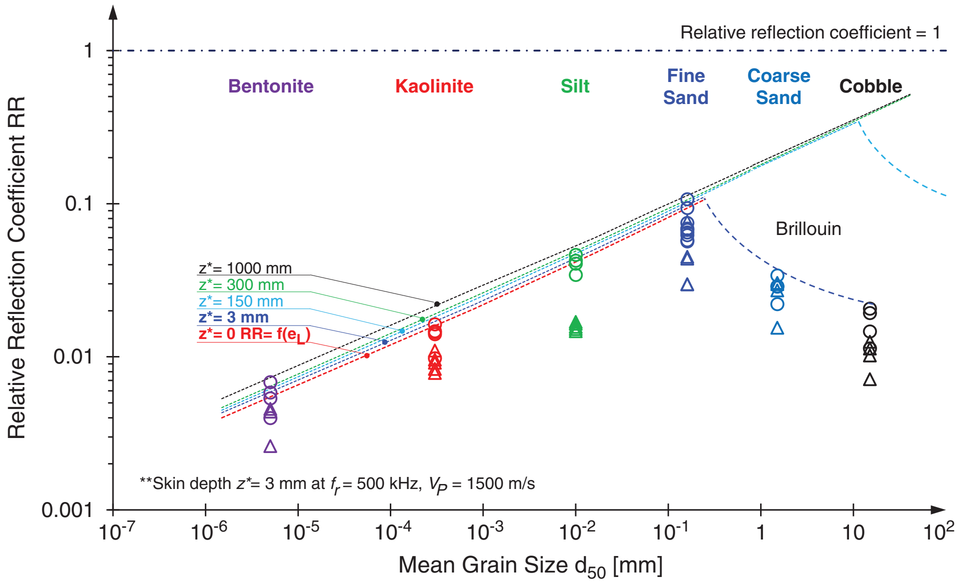

Fig. 11. (Color) Energy-based relative reflection coefficient RR for five different sediments versus mean grain size d_{50} in logarithmic scale. Table 1 summarizes the sediment properties. The relative reflection coefficient is $RR = E_s/E_{st}$ [Eq. (11)]—circles: data measured with high-damping transducer; triangles: data measured with low-damping transducer; dotted lines: theoretically computed relative reflection coefficient for six *reference sediments* at four different depths $z^* = 3$, 150, 300, and 1,000 mm [Eq. (11)]. Refer to Figs. 2(b) and 7 for sediment density ρ_s and P-wave velocity V_P. Steel: $V_P = 5{,}900$ m/s, $\rho = 7{,}900$ kg/m^3; water: $V_P = 1{,}531$ m/s, $\rho = 1{,}024$ kg/m^3. The lower red line is estimated in terms of void ratio e_L for the six reference sediments.

for silts and sands where the slope between the reflectivity and grain size is about $1/4$ in log-log scale.

Asymptotic Void Ratio

The previously discussed bathymetric study shows that the mass density ρ_o at very low effective stress $\sigma_z' \to 0$ is the critical parameter for high-frequency seafloor reflection studies (leveled seafloor). The ρ_o corresponds to the asymptotic void ratio e_L [Eq. (4)]:

$$\rho_o = \rho_w \left[\frac{S_G + e_L}{1 + e_L}\right] \text{(at depth } z = 0) \qquad (12)$$

Furthermore, the shear stiffness vanishes at $\sigma_z' = 0$ and $V_S = 0$. Then the P-wave velocity V_P at $z = 0$ becomes [Eq. (9)]

$$V_p(z=0) = \sqrt{\frac{B_s}{\rho_s}} = \sqrt{\left[\left(\frac{\rho_m + \rho_w e_L}{1 + e_L}\right) \cdot \left(\frac{\frac{e_L}{1+e_L}}{B_w} + \frac{1 - \frac{e_L}{1+e_L}}{B_m}\right)\right]^{-1}} \qquad (13)$$

Finally, RR is a function of the asymptotic void ratio e_L [After Eq. (11)]:

$$RR = 1.14 \times \left[1 - 2 \cdot \left(\sqrt{\frac{S_G + e_L}{\frac{B_w}{B_m} + e_L}} + 1\right)^{-1}\right]^2 \qquad (14)$$

Eq. (14) corresponds to the line for $z^* = 0$ in Fig. 11. The relative reflection coefficients measured with the low-frequency and low-damping transducer are lower owing to the longer wavelength. In all cases, the asymptotic void ratio e_L for the six reference sediments successfully anticipates the lower bound for RR.

Clearly, the asymptotic void ratio e_L emerges as an important parameter, both for self-compaction and for the stiffness evolution with depth. The asymptotic void ratio e_L is inversely proportional to the median grain size d_{50} in clays and silts (due to the prevalent role of interparticle electrical forces) and is affected by pore fluid chemistry [see data in Mesri and Olson (1971), Studds et al. (1998), and Stewart et al. (2003)]. On the other hand, the asymptotic void ratio e_L is geometry-controlled by granular packings in sands and gravels. In fact, data in Table 1 for the six selected reference sediments suggest $e_L = 0.4 \cdot [1 + (d_{50}/\text{mm})^{-0.28}]$. For comparison, this equation agrees well with the central trend in Jackson and Richardson (2007), though their data are limited to $d_{50} = 10^{-3}$ to 1 mm). Admittedly, very high-plasticity clays can form stable slurries at higher void ratios in freshwater (Liu and Santamarina 2018); however, a skeleton capable of shear wave transmission is first detected at void ratios similar to e_L values used in this paper. Overall, this analysis suggests the potential use of reflection data to estimate the asymptotic void ratio e_L and to infer the sediment type.

Sediment Classification—Nomenclature

Semiempirical seabed classification methods that rely on low-perturbation acoustic reflection measurements exhibit large variations (Bachman 1985; Leblanc 1992; Panda et al. 1994). Factors such as surface roughness, bioturbation, and variability contribute to data scatter (Jackson and Briggs 1992; Jackson et al. 1996; Clarke 1994; Lyons and Orsi 1998; Jackson and Richardson 2007). Several commercially available software packages attempt to create seafloor backscatter mosaics (e.g., Fledermaus by QPS). Analyses advanced in this study support and extend these efforts by providing mutually compatible geotechnical and geoacoustic properties.

Sediment classification requires more information than what can be extracted from acoustic data. Therefore, acoustic seafloor surveys and sediment sampling combine to provide robust spatial distributions of seafloor sediment types (Goff et al. 2004). Sediment classification for engineering purposes helps engineers anticipate the sediment properties and behavior by grouping them into similar engineering response categories (Casagrande 1948; Kulhawy and Chen 2009). Unfortunately, current marine sediment classifications use a 50% fraction to separate sand from silt or clay (Shepard 1954; Folk et al. 1970; Flemming 2000). Indeed, the 50% boundary does

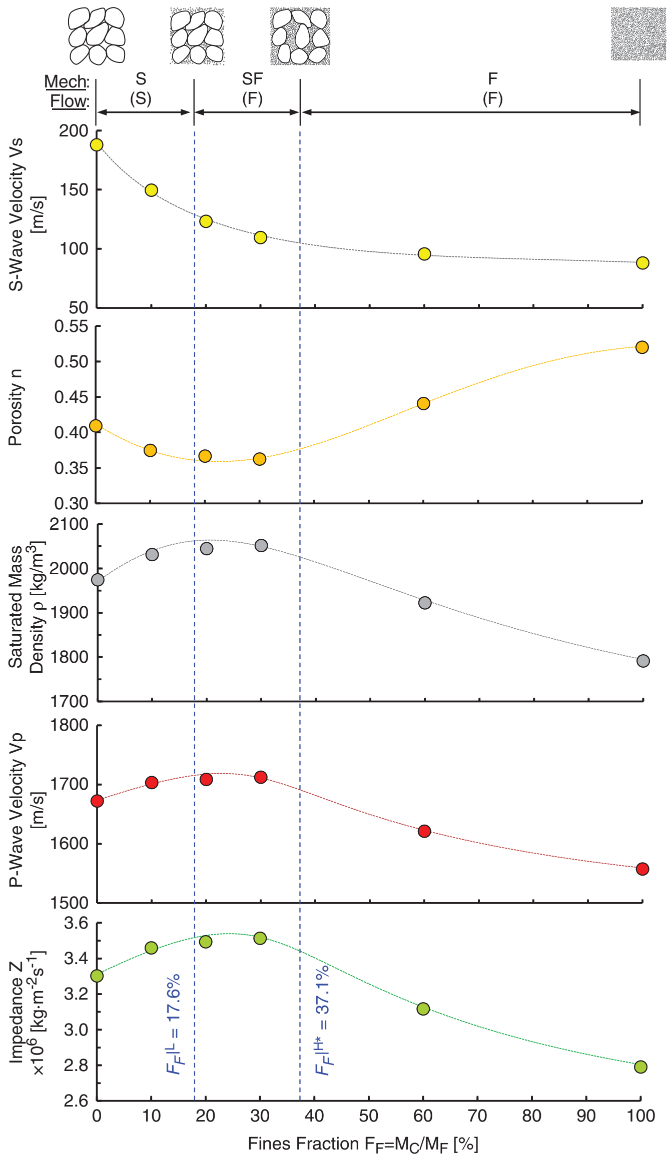

Fig. 12. (Color) Geoacoustic properties of sand–fines mixtures versus fines mass fraction F_F. The RSCS defines the component(s) responsible for mechanical behavior and fluid flow (top). Data points for S-wave velocity V_S at vertical effective stress $\sigma_z' = 15$ kPa and porosity from Park (2018). Saturated mass density, P-wave velocity V_P, and impedance Z are estimated from Eqs. (4) and (9). Input parameters used to compute RSCS boundaries $F_F|^L$ and $F_F|^{H^*}$ are for sand: $e_C^{max} = 0.78$ and $e_C^{min} = 0.53$; and for silt: $e_F^{max} = 1.50$ and $e_F^{min} = 0.73$.

not capture the transition from coarse-controlled to fines-controlled sediment behavior.

The newly revised soil classification system (RSCS) overcomes this limitation and classifies sediments as sand-controlled, transitional, or fines-controlled (Park and Santamarina 2017; Park et al. 2018); in particular, the RSCS captures the critical role of the fines fraction on geoacoustic properties. This is demonstrated with sand–silt mixtures in Fig. 12, where porosity, S- and P-wave velocities, and acoustic impedance data support the transition boundaries predicted by the RSCS: geoacoustic properties are sand-controlled up to a fines fraction of $F_F \approx 18\%$ and become clay-controlled when the fines fraction exceeds $F_F \approx 37\%$. Transition boundaries shift to lower fines contents F_F for higher-plasticity fines. Furthermore, sediment analyses must consider the salt concentration in pore fluid when sediments are classified with a letter F in the RSCS triangular textural chart (Jang and Santamarina 2016, 2017).

Conclusions

This study highlights the close relationship between sediment type, self-compaction, and geoacoustic properties with depth. Therefore, geoacoustic profiles and bathymetric data can be used to acquire insightful information about seafloor sediments and to anticipate their engineering properties. Important conclusions of the study are as follows:

- The asymptotically correct exponential compaction model provides a robust fit to porosity n and density ρ_s depth profiles as a function of effective stress σ_z'. The asymptotic void ratio at low effective stress e_L determines the sediment density ρ_o at the sediment–water boundary. The sediment specific-surface and sedimentation conditions define the value of e_L.
- The effective stress σ_z' determines the depth-dependent shear stiffness G_s, often augmented by synsedimentary or postsedimentary diagenesis. Shear stiffness vanishes as the sediment depth $z \to 0$ and $\sigma_z' \to 0$. The Biot-Gassmann P-wave velocity estimated for zero shear stiffness (i.e., $V_S = 0$) provides a lower bound for the P-wave velocity of near-surface seafloor sediments.
- A group of *reference sediments* that range from clean sands to high-plasticity clays was identified. Predicted void ratio, P-wave velocity V_P, and S-wave velocity V_S trends computed for these reference sediments capture prevalent trends observed in a large data set compiled from the literature and from a focused laboratory study conducted as part of this study.
- The measured high-frequency reflection coefficient *RR* (relative to a steel reflector at the same depth) and the computed reflection coefficient for the selected reference sediments show distinct sediment-dependent reflectivity. In fact, the asymptotic density ρ_o at zero effective stress defines the acoustic reflection amplitude for high-frequency applications, such as bathymetric imaging.
- Model parameters for compaction and stiffness must be congruent. Model parameters adopted for the selected reference sediments reflect correlations reported in the literature in terms of specific surface, plasticity, and grain characteristics.
- The proposed analysis of geoacoustic data can be used to gain first-order estimates of the seafloor sediment properties and to produce sediment-type seafloor maps.

Data Availability Statement

All data, models, and algorithms generated or used during the study appear in the published article.

Acknowledgments

Support for this research was provided by the KAUST Endowment at King Abdullah University of Science and Technology. Gabrielle E. Abelskamp edited the manuscript.

Notation

The following symbols are used in this paper:

a = slenderness ratio;
B = bulk modulus;

C_c = compression index;
C_u = coefficient of uniformity;
D_r = relative density;
d_{50} = median grain size;
dz = differential of depth;
E = energy;
e = void ratio;
f_r = operating frequency;
G_s = sediment shear stiffness;
g = gravity;
n = porosity;
RR = relative reflection coefficient;
R^* = roundness;
S_G = specific gravity;
V_p = P-wave velocity;
$V_{P\infty}$ = high-frequency P-wave velocity;
V_{Po} = low frequency P-wave velocity;
V_s = S-wave velocity;
Z = impedance;
z = depth;
α = shear wave velocity at $\sigma_z' = 1$ kPa;
β = sensitivity of shear wave velocity to effective stress;
λ = wavelength;
ρ = mass density;
ξ = tortuosity factor;
ω = water content;
η = compaction model parameter;
σ_z' = vertical effective stress;
σ_c' = characteristic effective stress; and
ν_{sk} = small-strain Poisson's ratio of soil skeleton.

Subscripts

H = at $\sigma_z' \to \infty$, z = at depth z;
m = mineral;
sk = granular skeleton;
s = sediment;
st = steel;
w = water;
0 = sediment at $z = 0$;
1 kPa = at $\sigma_z' = 1$ kPa; and
L = at $\sigma_z' \to 0$.

References

Ali, H. B., and M. K. Broadhead. 1995. "Shear wave properties from inversion of Scholte wave data." In *Full field inversion methods in ocean and seismo-acoustics*, 371–376. Dordrecht, Netherlands: Springer.

Andrén, T., B. B. Jørgensen, C. Cotterill, and S. Green. 2015a. "The IODP expedition 347 scientific party." In Vol. 347 of *Proc., Integrated Ocean Drilling Program, Site M0059*. Washington, DC: Integrated Ocean Drilling Program Management International. https://doi.org/10.2204/iodp.proc.347.103.2015.

Andrén, T., B. B. Jørgensen, C. Cotterill, and S. Green. 2015b. "The IODP expedition 347 scientific party." In Vol. 347 of *Proc., Integrated Ocean Drilling Program, Site M0060*. Washington, DC: Integrated Ocean Drilling Program Management International. https://doi.org/10.2204/iodp.proc.347.104.2015.

Andrén, T., B. B. Jørgensen, C. Cotterill, and S. Green. 2015c. "The IODP expedition 347 scientific party." In Vol. 347 of *Proc., Integrated Ocean Drilling Program, Site M0063*. Washington, DC: Integrated Ocean Drilling Program Management International. https://doi.org/10.2204/iodp.proc.347.107.2015.

Bachman, R. T. 1985. "Acoustic and physical property relationships in marine sediment." *J. Acoust. Soc. Am.* 78 (2): 616–621. https://doi.org/10.1121/1.392429.

Bibee, L. D., and L. M. Dorman. 1995. "Full waveform inversion of seismic interface wave data." In *Full field inversion methods in ocean and seismo-acoustics*, 377–382. Dordrecht, Netherlands: Springer.

Briggs, K. B. 1994. "High-frequency acoustic scattering from sediment interface roughness and volume inhomogeneities." Ph.D. dissertation, School of Marine and Atmospheric Science, Univ. of Miami.

Buchanan, J. L. 2005. *An assessment of the Biot-Stoll model of a poroelastic seabed*. Rep. No. NRL/MR/7140–05-8885. Washington DC: Acoustic Signal Processing Branch.

Buckingham, M. J. 2005. "Compressional and shear wave properties of marine sediments: Comparisons between theory and data." *J. Acoust. Soc. Am.* 117 (1): 137–152. https://doi.org/10.1121/1.1810231.

Burland, J. B. 1990. "On the compressibility and shear strength of natural clays." *Géotechnique* 40 (3): 329–378. https://doi.org/10.1680/geot.1990.40.3.329.

Caiti, A., T. Akal, and R. D. Stoll. 1991. "Determination of shear velocity profiles by inversion of interface wave data." In *Shear waves in marine sediments*, 557–565. Dordrecht, Netherlands: Springer.

Caiti, A., T. Akal, and R. D. Stoll. 1994. "Estimation of shear wave velocity in shallow marine sediments." *IEEE J. Oceanic Eng.* 19 (1): 58–72. https://doi.org/10.1109/48.289451.

Carter, R. M., I. N. McCave, C. Richter, and L. Carter. 1999. "Leg 181 Summary: Southwest Pacific paleoceanography." In *Proc. Ocean Drill. Program, A, Initial Rep. 181*. College Station, TX: Ocean Drilling Program, Texas A&M Univ.

Casagrande, A. 1948. "Classification and identification of soils." *Trans. ASCE* 113 (1): 901–930.

Cha, M., J. C. Santamarina, H. S. Kim, and G. C. Cho. 2014. "Small-strain stiffness, shear-wave velocity, and soil compressibility." *J. Geotech. Geoenviron. Eng.* 140 (10): 06014011. https://doi.org/10.1061/(ASCE)GT.1943-5606.0001157.

Cho, G. C., J. Dodds, and J. C. Santamarina. 2006. "Particle shape effects on packing density, stiffness, and strength: Natural and crushed sands." *J. Geotech. Geoenviron. Eng.* 132 (5): 591–602. https://doi.org/10.1061/(ASCE)1090-0241(2006)132:5(591).

Chong, S. H., and J. C. Santamarina. 2016. "Soil compressibility models for a wide stress range." *J. Geotech. Geoenviron. Eng.* 142 (6): 06016003. https://doi.org/10.1061/(ASCE)GT.1943-5606.0001482.

Clarke, J. H. 1994. "Toward remote seafloor classification using the angular response of acoustic backscattering: A case study from multiple overlapping GLORIA data." *IEEE J. Ocean. Eng.* 19 (1): 112–127. https://doi.org/10.1109/48.289456.

Cunny, R. W., and Z. B. Fry. 1973. "Vibratory in situ and laboratory soil moduli compared." *J. Geotech. Geoenviron. Eng.* 99 (12): 1055–1076.

Davis, E. E., et al. 1992a. "Site 857." In Vol. 857 of *Proc., Ocean Drilling Program, Initial Reports, 139*, 283–429. College Station, TX: Ocean Drilling Program, Texas A&M Univ. https://doi.org/10.2973/odp.proc.ir.139.107.1992.

Davis, E. E., et al. 1992b. "Site 858." In Vol. 858 of *Proc., Ocean Drilling Program, Initial Reports, 139*, 431–569. College Station, TX: Ocean Drilling Program, Texas A&M Univ. https://doi.org/10.2973/odp.proc.ir.139.108.1992.

Day, R. W. 2000. *Geotechnical engineer's portable handbook*. New York: McGraw-Hill.

D'Hondt, S., F. Inagaki, and C. A. Alvarez Zarikian. 2011. "The expedition 329 scientists."In *Proc. IODP, 329*. Tokyo: Integrated Ocean Drilling Program Management International. https://doi.org/10.2204/iodp.proc.329.112.2011.

D'Hondt, S. L., et al. 2003. "Site 1226." In *Proc. ODP, Init. Repts., 201*, edited by S. L. D'Hondt, B. B. Jørgensen, D. J. Miller, et al., 1–96. College Station, TX: Ocean Drilling Program, Texas A&M Univ: Ocean Drilling Program. https://doi.org/10.2973/odp.proc.ir.201.107.2003.

Feary, D. A., A. C. Hine, and M. J. Malone. 2000. In *Proceedings of ODP: Ocean Drilling Program. Initial Reports, 182*. College Station, TX: Ocean Drilling Program, Texas A&M Univ.

Ferdelman, T. G., A. Kano, T. Williams, and J.-P. Henriet. 2006. "The Expedition 307 Scientists. Site U1316." In *Proc. IODP, 307*: Washington, DC: Integrated Ocean Drilling Program Management International. https://doi.org/10.2204/iodp.proc.307.103.2006.

Fisher, A. T., T. Urabe, and A. Klaus. 2005. "The Expedition 301 Scientists. Site U1301." In *Proc. IODP, 301*. College Station, TX: Integrated Ocean Drilling Program Management International. https://doi.org/10.2204/iodp.proc.301.106.2005.

Flemming, B. W. 2000. "A revised textural classification of gravel-free muddy sediments on the basis of ternary diagrams." *Cont. Shelf Res.* 20 (10–11): 1125–1137. https://doi.org/10.1016/S0278-4343(00)00015-7.

Folk, R. L., P. B. Andrews, and D. W. Lewis. 1970. "Detrital sedimentary rock classification and nomenclature for use in New Zealand." *N. Z. J. Geol. Geophys.* 13 (4): 937–968. https://doi.org/10.1080/00288306.1970.10418211.

Gabriels, P., R. Snieder, and G. Nolet. 1987. "In situ measurements of shear-wave velocity in sediments with higher-mode Rayleigh waves." *Geophys. Prospect.* 35 (2): 187–196. https://doi.org/10.1111/j.1365-2478.1987.tb00812.x.

Giao, P. H., N. T. Dung, and P. V. Long. 2008. "An integrated geotechnical–geophysical investigation of soft clay at a coastal site in the Mekong Delta for oil and gas infrastructure development." *Can. Geotech. J.* 45 (11): 1514–1524. https://doi.org/10.1139/T08-077.

Goff, J. A., B. J. Kraft, L. A. Mayer, S. G. Schock, C. K. Sommerfield, H. C. Olson, S. P. Gulick, and S. Nordfjord. 2004. "Seabed characterization on the New Jersey middle and outer shelf: Correlatability and spatial variability of seafloor sediment properties." *Mar. Geol.* 209 (1–4): 147–172. https://doi.org/10.1016/j.margeo.2004.05.030.

Goldhammer, R. K. 1997. "Compaction and decompaction algorithms for sedimentary carbonates." *J. Sediment. Res.* 67 (1): 26–35.

Grant, J. A., and R. Schreiber. 1990. "Modern swathe sounding and sub-bottom profiling technology for research applications: The Atlas Hydrosweep and Parasound systems." In *Marine geological surveying and sampling*, 9–19. Dordrecht, Netherlands: Springer.

Gregory, A. S., W. R. Whalley, C. W. Watts, N. R. A. Bird, P. D. Hallett, and A. P. Whitmore. 2006. "Calculation of the compression index and precompression stress from soil compression test data." *Soil Tillage Res.* 89 (1): 45–57. https://doi.org/10.1016/j.still.2005.06.012.

Hamilton, E. L. 1972. "Compressional-wave attenuation in marine sediments." *Geophysics* 37 (4): 620–646. https://doi.org/10.1190/1.1440287.

Hamilton, E. L. 1976. "Shear-wave velocity versus depth in marine sediments: A review." *Geophysics* 41 (5): 985–996. https://doi.org/10.1190/1.1440676.

Hamilton, E. L. 1979. "Vp/Vs and Poisson's ratios in marine sediments and rocks." *J. Acoust. Soc. Am.* 66 (4): 1093–1101. https://doi.org/10.1121/1.383344.

Hamilton, E. L., and R. T. Bachman. 1982. "Sound velocity and related properties of marine sediments." *J. Acoust. Soc. Am.* 72 (6): 1891–1904. https://doi.org/10.1121/1.388539.

Holzer, T. L., M. J. Bennett, T. E. Noce, and J. C. Tinsley. 2005. "Shear-wave velocity of surficial geologic sediments in northern California: Statistical distributions and depth dependence." *Earthquake Spectra* 21 (1): 161–177. https://doi.org/10.1193/1.1852561.

Hong, Z. S., L. L. Zeng, Y. J. Cui, Y. Q. Cai, and C. Lin. 2012. "Compression behaviour of natural and reconstituted clays." *Géotechnique* 62 (4): 291–301. https://doi.org/10.1680/geot.10.P.046.

Inagaki, F., M. Suzuki, K. Takai, H. Oida, T. Sakamoto, K. Aoki, K. H. Nealson, and K. Horikoshi. 2003. "Microbial communities associated with geological horizons in coastal subseafloor sediments from the Sea of Okhotsk." *Appl. Environ. Microbiol.* 69 (12): 7224–7235. https://doi.org/10.1128/AEM.69.12.7224-7235.2003.

Jackson, D. R., and K. B. Briggs. 1992. "High-frequency bottom backscattering: Roughness versus sediment volume scattering." *J. Acoust. Soc. Am.* 92 (2): 962–977. https://doi.org/10.1121/1.403966.

Jackson, D. R., K. B. Briggs, K. L. Williams, and M. D. Richardson. 1996. "Tests of models for high-frequency seafloor backscatter." *IEEE J. Ocean. Eng.* 21 (4): 458–470. https://doi.org/10.1109/48.544057.

Jackson, D. R., and M. D. Richardson. 2007. *High-frequency seafloor acoustics*. New York: Springer.

Jang, J., and J. C. Santamarina. 2016. "Fines classification based on sensitivity to pore-fluid chemistry." *J. Geotech. Geoenviron. Eng.* 142 (4): 06015018. https://doi.org/10.1061/(ASCE)GT.1943-5606.0001420.

Jang, J., and J. C. Santamarina. 2017. "Fines classification based on sensitivity to pore-fluid chemistry." *J. Geotech. Geoenviron. Eng.* 142 (4): 07017013. https://doi.org/10.1061/(ASCE)GT.1943-5606.0001694.

Johns, M. W. 1986. *Consolidation and permeability characteristics of Japan Trench and Nankai Trough sediments from Deep Sea Drilling Project Leg 87*. College Station, TX: Deep Sea Drilling Project, Texas A&M Univ.

Kang, X., G. C. Kang, and B. Bate. 2014. "Measurement of stiffness anisotropy in kaolinite using bender element tests in a floating wall consolidometer." *Geotech. Test. J.* 37 (5): 869–883. https://doi.org/10.1520/GTJ20120205.

Keller, G. H., and R. H. Bennett. 1973. *Sediment mass physical properties—Panama basin and northeastern equatorial pacific*. Initial Reports of the Deep Sea Drilling Project, 499–512. College Station, TX: Deep Sea Drilling Project, Texas A&M Univ.

Kjaernsli, B. and A. Sande. 1963. "Compressibility of some coarse-grained materials." In Vol. 1 of *Proc., 1st European Conf. on Soil Mechanics and Foundation Engineering*, 245–251. Budapest: Akad. Kiadó.

Klein, K., and J. C. Santamarina. 2005. "Soft sediments: Wave-based characterization." *Int. J. Geomech.* 5 (2): 147–157. https://doi.org/10.1061/(ASCE)1532-3641(2005)5:2(147).

Kominz, M., K. Patterson, and D. Odette. 2011. "Lithology dependence of porosity in slope and deep marine sediments." *J. Sediment. Res.* 81 (10): 730–742. https://doi.org/10.2110/jsr.2011.60.

Ku, T. 2012. "Geostatic stress state evaluation by directional shear wave velocities, with application towards geocharacterization at Aiken, SC." Ph.D. thesis, School of Civil and Environmental Engineering, Georgia Institute of Technology.

Ku, T., S. Subramanian, S. W. Moon, and J. Jung. 2017. "Stress dependency of shear-wave velocity measurements in soils." *J. Geotech. Geoenviron. Eng.* 143 (2): 04016092. https://doi.org/10.1061/(ASCE)GT.1943-5606.0001592.

Kulhawy, F. H., and J. R. Chen. 2009. "Identification and description of soils containing very coarse fractions." *J. Geotech. Geoenviron. Eng.* 135 (5): 635–646. https://doi.org/10.1061/(ASCE)1090-0241(2009)135:5(635).

Leblanc, L. R. 1992. "Sonar attenuation modeling for classification of marine sediments." *J. Acoust. Soc. Am.* 91 (1): 116–126. https://doi.org/10.1121/1.402759.

Lee, J. S., C. Lee, H. K. Yoon, and W. Lee. 2010. "Penetration type field velocity probe for soft soils." *J. Geotech. Geoenviron. Eng.* 136 (1): 199–206. https://doi.org/10.1061/(ASCE)1090-0241(2010)136:1(199).

Lee, J. S., and J. C. Santamarina. 2005a. "Bender elements: Performance and signal interpretation." *J. Geotech. Geoenviron. Eng.* 131 (9): 1063–1070. https://doi.org/10.1061/(ASCE)1090-0241(2005)131:9(1063).

Lee, J. S., and J. C. Santamarina. 2005b. "P-wave reflection imaging." *Geotech. Test. J.* 28 (2): 197–206.

Leroueil, S. 1996. "Compressibility of clays: Fundamental and practical aspects." *J. Geotech. Eng.* 122 (7): 534–543. https://doi.org/10.1061/(ASCE)0733-9410(1996)122:7(534).

Liu, H. P., Y. Hu, J. Dorman, T. S. Chang, and J. M. Chiu. 1997. "Upper Mississippi embayment shallow seismic velocities measured in situ." *Eng. Geol.* 46 (3–4): 313–330. https://doi.org/10.1016/S0013-7952(97)00009-4.

Liu, Q., and J. C. Santamarina. 2018. "Mudcake growth: Model and implications." *J. Petrol. Sci. Eng.* 162 (Mar): 251–259. https://doi.org/10.1016/j.petrol.2017.12.044.

Lovell, M. A., and P. Ogden. 1984. *Remote assessment of permeability/thermal diffusivity of consolidated clay sediments*. Rep. No. EUR–9206. Luxembourg: Directorate-General Science. Research and Development.

Lyons, A. P., and T. H. Orsi. 1998. “The effect of a layer of varying density on high-frequency reflection, forward loss, and backscatter.” *IEEE J. Ocean. Eng.* 23 (4): 411–422. https://doi.org/10.1109/48.725235.

Mesri, G., and R. E. Olson. 1971. “Consolidation characteristics of montmorillonite.” *Géotechnique* 21 (4): 341–352. https://doi.org/10.1680/geot.1971.21.4.341.

Moore, G. F., et al. 2001a. “Shipboard scientific party: Site 1174.” In Vol. 190 of *Proc. ODP.* Initial Rep., 1–149. College Station, TX: Ocean Drilling Program. https://doi.org/10.2973/odp.proc.ir.190.105.2001.

Moore, G. F., et al. 2001b. “Shipboard scientific party, 2001: Site 1178.” In Vol. 190 of *Proc. ODP.* Initial Rep., 1–108. College Station, TX: Ocean Drilling Program. https://doi.org/10.2973/odp.proc.ir.190.109.2001.

Moridis, G. J., et al. 2011. “Challenges, uncertainties, and issues facing gas production from gas-hydrate deposits.” *SPE Reservoir Eval. Eng.* 14 (1): 76–112. https://doi.org/10.2118/131792-PA.

Mottl, M. J., et al. 1994. “Site 858.” In Vol. 139 of *Proc., Ocean Drilling Program, Scientific Results, Middle Valley, Juan de Fuca Ridge*. College Station, TX: Ocean Drilling Program, Texas A&M Univ.

Muir, T. G., A. Caiti, J. M. Hovem, T. Akal, M. D. Richardson, and R. D. Stoll. 1991. “Comparison of techniques for shear wave velocity and attenuation measurements.” In *Shear waves in marine sediments*, 283–294. Dordrecht, Netherlands: Springer.

Nowamooz, H., and F. Masrouri. 2009. “Density-dependent hydromechanical behaviour of a compacted expansive soil.” *Eng. Geol.* 106 (3–4): 105–115. https://doi.org/10.1016/j.enggeo.2009.03.010.

Palomino, A. M., and J. C. Santamarina. 2005. “Fabric map for kaolinite: Effects of pH and ionic concentration on behavior.” *Clays Clay Miner.* 53 (3): 211–223. https://doi.org/10.1346/CCMN.2005.0530302.

Panda, S., L. R. LeBlanc, and S. G. Schock. 1994. “Sediment classification based on impedance and attenuation estimation.” *J. Acoust. Soc. Am.* 96 (5): 3022–3035. https://doi.org/10.1121/1.411266.

Park, J. 2018. “Long-term response of soils subjected to repetitive mechanical loads: Engineering implications.” Ph.D. thesis, School of Civil and Environmental Engineering, Georgia Institute of Technology.

Park, J., G. M. Castro, and J. C. Santamarina. 2018. “Revised soil classification system for coarse-fine mixtures.” *J. Geotech. Geoenviron. Eng.* 143 (8): 07018019. https://doi.org/10.1061/(ASCE)GT.1943-5606.0001908.

Park, J., and J. C. Santamarina. 2017. “Revised soil classification system for coarse-fine mixtures.” *J. Geotech. Geoenviron. Eng.* 143 (8): 04017039. https://doi.org/10.1061/(ASCE)GT.1943-5606.0001705.

Parson, L., et al. 1992. “Shipboard scientific party, 1992: Site 834.” In Vol. 135 of *Proc. ODP*, Initial Rep., 85–180. College Station, TX: Ocean Drilling Program. https://doi.org/10.2973/odp.proc.ir.135.104.1992.

Pestana, J. M., and A. J. Whittle. 1995. “Compression model for cohesionless soils.” *Géotechnique* 45 (4): 611–631. https://doi.org/10.1680/geot.1995.45.4.611.

Richardson, M. D., and K. B. Briggs. 1993. “On the use of acoustic impedance values to determine sediment properties.” *Proc. Inst. Acoust.* 15: 15–23.

Richardson, M. D., E. Muzi, B. Miaschi, and F. Tugutcan. 1991. “Shear wave gradients in near-surface marine sediments.” In *Shear waves in marine sediments*, 295–304. Dordrecht, Netherlands: Kluwer.

Roesler, S. K. 1979. “Anisotropic shear modulus due to stress anisotropy.” *J. Geotech. Eng. Div.* 105 (7): 871–880.

Santamarina, J. C., and G. C. Cho. 2004. “Soil behaviour: The role of particle shape.” In Vol. 1 of *Proc., Advances in Geotechnical Engineering: The Skempton Conf.*, edited by R. J. Jardine, D. M. Potts, and K. G. Higgins, 604–617. London: Thomas Telford.

Santamarina, J. C., K. A. Klein, and M. A. Fam. 2001. *Soils and waves: Particulate materials behavior, characterization and process monitoring*. New York: Wiley.

Sauter, A. W. 1987. “Studies of the upper oceanic floor using ocean bottom seismometers.” Ph.D. dissertation, Scripps Institution of Oceanography, Univ. of California San Diego.

Schrottke, K., M. Becker, A. Bartholomä, B. W. Flemming, and D. Hebbeln. 2006. “Fluid mud dynamics in the Weser estuary turbidity zone tracked by high-resolution side-scan sonar and parametric sub-bottom profiler.” *Geo-Mar. Lett.* 26 (3): 185–198. https://doi.org/10.1007/s00367-006-0027-1.

Schultheiss, P. J. 1981. “Simultaneous measurement of P & S wave velocities during conventional laboratory soil testing procedures.” *Mar. Georesour. Geotech.* 4 (4): 343–367. https://doi.org/10.1080/10641198109379831.

Shepard, F. P. 1954. “Nomenclature based on sand-silt-clay ratios.” *J. Sediment. Petrol.* 24 (3): 151–158.

Snellen, M., K. Siemes, and D. G. Simons. 2011. “Model-based sediment classification using single-beam echosounder signals.” *J. Acoust. Soc. Am.* 129 (5): 2878–2888. https://doi.org/10.1121/1.3569718.

Sternlicht, D. D., and C. P. de Moustier. 2003. “Remote sensing of sediment characteristics by optimized echo-envelope matching.” *J. Acoust. Soc. Am.* 114 (5): 2727–2743. https://doi.org/10.1121/1.1608019.

Stewart, D. I., P. G. Studds, and T. W. Cousens. 2003. “The factors controlling the engineering properties of bentonite-enhanced sand.” *Appl. Clay Sci.* 23 (1–4): 97–110. https://doi.org/10.1016/S0169-1317(03)00092-9.

Stoll, R. D., G. M. Bryan, R. Mithal, and R. Flood. 1991. “Field experiments to study seafloor seismoacoustic response.” *J. Acoust. Soc. Am.* 89 (5): 2232–2240. https://doi.org/10.1121/1.400915.

Studds, P. G., D. I. Stewart, and T. W. Cousens. 1998. “The effects of salt solutions on the properties of bentonite-sand mixtures.” *Clay Miner.* 33 (4): 651–660. https://doi.org/10.1180/claymin.1998.033.4.12.

Takai, K., M. J. Mottl, S. H. Nielsen, and the Expedition 331 Scientists. 2011. “Site C0013.” In *Proc. IODP, 331*. Tokyo: Integrated Ocean Drilling Program Management International. https://doi.org/10.2204/iodp.proc.331.103.2011.

Taylor, B., P. Huchon, and A. Klaus. 1999. In vol. 180 of *Proc., Ocean Drilling Program*. College Station, TX: Ocean Drilling Program, Texas A&M Univ. https://doi.org/10.2973/odp.proc.ir.180.105.2000.

Terzariol, M., J. Park, G. M. Castro, and J. C. Santamarina. 2020. “Methane hydrate-bearing sediments: Pore habit and implications.” *Mar. Pet. Geol.* 116: 104302.

Van Walree, P. A., M. A. Ainslie, and D. G. Simons. 2006. “Mean grain size mapping with single-beam echo sounders.” *J. Acoust. Soc. Am.* 120 (5): 2555–2566. https://doi.org/10.1121/1.2345907.

Van Walree, P. A., J. Tęgowski, C. Laban, and D. G. Simons. 2005. “Acoustic seafloor discrimination with echo shape parameters: A comparison with the ground truth.” *Cont. Shelf Res.* 25 (18): 2273–2293. https://doi.org/10.1016/j.csr.2005.09.002.

Wang, Y., and Y. Rao. 2009. “Reflection seismic waveform tomography.” *J. Geophys. Res. Solid Earth* 114 (B3): WCC1–WCC26. https://doi.org/10.1029/2008JB005916.

Wang, Y. H., and W. K. Siu. 2006. “Structure characteristics and mechanical properties of kaolinite soils. I. Surface charges and structural characterizations.” *Can. Geotech. J.* 43 (6): 587–600. https://doi.org/10.1139/t06-026.

Wang, Y. H., and D. Xu. 2007. “Dual porosity and secondary consolidation.” *J. Geotech. Geoenviron. Eng.* 133 (7): 793–801. https://doi.org/10.1061/(ASCE)1090-0241(2007)133:7(793).

Wunderlich, J., G. Wendt, and S. Müller. 2005. “High-resolution echosounding and detection of embedded archaeological objects with nonlinear sub-bottom profilers.” *Mar. Geophys. Res.* 26 (2–4): 123–133. https://doi.org/10.1007/s11001-005-3712-y.

Yoon, H. K., and J. S. Lee. 2010. “Field velocity resistivity probe for estimating stiffness and void ratio.” *Soil Dyn. Earthquake Eng.* 30 (12): 1540–1549. https://doi.org/10.1016/j.soildyn.2010.07.008.

Youd, T. L. 1973. “Factors controlling maximum and minimum densities of sands.” *ASTM Spec. Tech. Publ.* 523: 98–112.